International Conference on Nuclear Data for Science and Technology 2007
DOI: 10.1051/ndata:07625

A new measurement of the H(n,n)H elastic scattering angular distribution at 14.9 MeV

Nourredine Boukharouba[1,a], Thomas N. Massey[2], Robert C. Haight[3], Steven M. Grimes[2], Donald E. Carter[4], Allan D. Carlson[5], Charles E. Brient[2], and Fred B. Bateman[5]

[1] Department of Physics, University of Guelma, Guelma 24000, Algeria
[2] Department of Physics and Astronomy, Ohio University, Athens, OH 45701, USA
[3] Los Alamos Neutron Science Center, Los Alamos National Laboratory, Los Alamos, NM 87545, USA
[4] Institute of Nuclear and Particle Physics, Ohio University, Athens, OH 45701, USA
[5] National Institute of Standards and Technology, 100 Bureau Dr., Stop 8463, Gaithersburg, MD 20899-8463, USA

Abstract. The relative angular distribution of the scattering of neutrons by protons was measured at E_n = 14.9 MeV neutron energy for center-of-mass scattering angles ranging from 60° to 180°. Absolute angular distribution values were obtained by normalizing the measured line shape to the accurately known n-p total cross section. Initial assessment indicates a somewhat better agreement of the data with the predictions of Arndt and Nijmegen than with the ENDF/B-VII.0 evaluation.

1 Introduction

Most measured data for n-p scattering in the 14 MeV neutron energy range are dated and not of a precision expected for such an important standard. In addition to large estimated uncertainties in individual measurements, these data sets differ significantly and are not in good agreement with the theoretical and evaluated data. Any calculation that uses this cross section as input, in this energy region, is bound to suffer from additional uncertainties in its results introduced by the lack of accuracy in the standard. We have undertaken a series of experiments to measure this cross section with greater accuracy than is currently available. A major improvement in the present measurement over previous ones was the larger angular range covered. Recoil protons were detected between 0° and 60° in the laboratory system resulting in a better determination of the angular distribution line shape. Further improvements came from the use of up-to-date electronics and computer systems to achieve cleaner recoil proton spectra with minimum dead time.

2 Experimental details

The experimental procedure consisted in counting recoil protons resulting from neutron bombardment of a 3.8 mg/cm^2-thick polypropylene foil. The detector system was made of 11 eleven ΔE-E telescopes located right and left of the neutron beam axis at 0°, ±12°, ±24°, ±36°, ±48° and ±60° in the laboratory system.

2.1 Experimental layout

The general layout of the scattering chamber and telescope system was previously described in detail in ref. [1] and is shown in figure 1. It was composed of a shielded multi-telescope scattering chamber housing the 11 ΔE-E telescopes located symmetrically on both sides of the beam axis to minimize systematic errors in angle determination and to provide redundant independent measurements. Detector thicknesses were optimized for the recoil proton energy available at each angle. Furthermore, the telescope system eliminates the necessity of accurate monitoring of the neutron beam intensity which was the case in a number of previous measurements where data were taken one angle at a time. Relative solid angle normalization was obtained by using a very thin and highly uniform ^{239}Pu α-source [1]. Neutrons were generated by deuteron bombardment of a tritiated target, collimated and directed onto a polypropylene foil mounted on a 0.5-mm tantalum backing. A wobbler is used to reduce heating in the tritiated target. An NE213 neutron detector with n-γ discrimination was utilized to normalize the incident neutron fluence of the different experimental runs in addition to a beam current integration apparatus. A further check of this normalization was provided by the (n,z) reaction in the 0° E-detector. There was an excellent agreement between these methods (less than

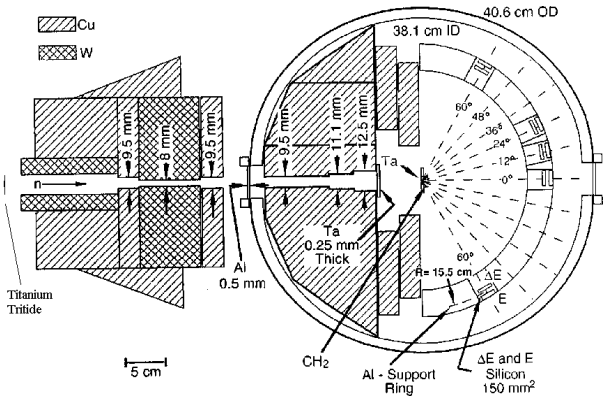

Fig. 1. Layout of the scattering chamber, neutron source, telescope system and shielding.

[a] Presenting author, e-mail: nboukhar@yahoo.fr

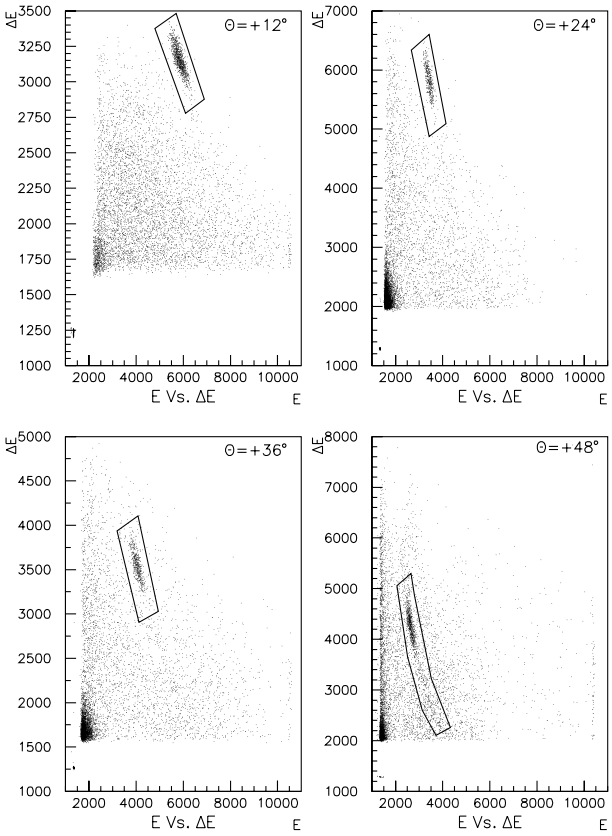

Fig. 2. E-ΔE scatter plots and typical regions of interest used to gate the event stream.

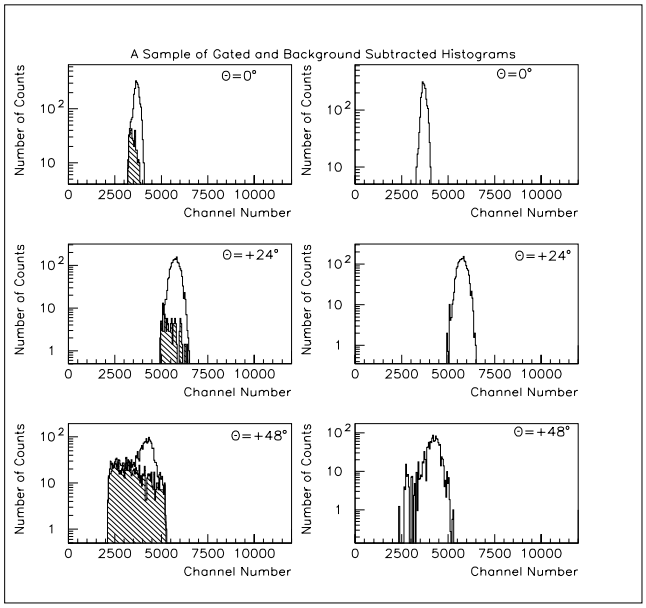

Fig. 3. Typical gated and background-corrected histograms. The graphs on the left-hand-side show an overlay of the background and the foreground on a log scale. The normalized background is shown in hatched style. The right-hand-side column shows the net background-corrected recoil proton peak.

0.3% difference). Background was estimated from sample-out runs that were taken in alternated fashion with the sample-in runs. The sample-out runs used a blank target consisting of a Ta backing without the polypropylene foil.

2.2 Data acquisition system

In order to minimize dead time problems and amplifier summing noise cross-talk, each individual telescope was handled separately by a dedicated data acquisition system (DAQ) consisting of a data acquisition board mounted in a separate independent personal computer. An additional data acquisition board and computer were used for the NE213 neutron monitor. A distributed DAQ [2] was thus achieved by connecting the 12 DAQ systems to a master personal computer to synchronize data acquisition start and stop times for all telescopes and the neutron monitor. Improved techniques for dead time determination were used [2]. Data was taken in event mode for later replay and analysis.

3 Data analysis, corrections and results

An initial check of the data consisted in replaying individual runs and computing their counting ratio per event file relative to telescope 2 for each telescope. This ratio should be fairly constant within statistical fluctuations for any given telescope. Any run that exhibited a significant deviation from the mean counting ratio was excluded from the data set used in the computation of the angular distribution. Significant amounts of data were thus eliminated from the final data set because of a counting instability problem.

3.1 Data reduction

E-ΔE scatter plots (fig. 2) were generated for each telescope from the corresponding event stream. Regions of interest were drawn around recoil protons and used subsequently to filter the event stream for both sample-in and sample-out runs. Proton yields were obtained for the gated foreground and background data and normalized using the NE213 neutron monitor. The normalized gated background was then subtracted from the sample-in data and net proton yields were obtained. Figure 3 shows a sample of background-corrected recoil proton histograms for 3 different telescopes. The effects of the E-ΔE gate size and shape were studied in detail. Wide gates were drawn around the recoil proton events and iteratively reduced in size until the net proton yield was stable and the background yield was lowest, thus minimizing uncertainties in the net proton yields due to gate size and shape.

3.2 Corrections

The relative solid angle normalization factors obtained from the α source were applied to the net proton yields. These factors are shown in figure 4. All but the 60° telescopes were fitted with similar circular solid-angle defining collimators located in front of the ΔE detectors. The 60° telescopes were equipped

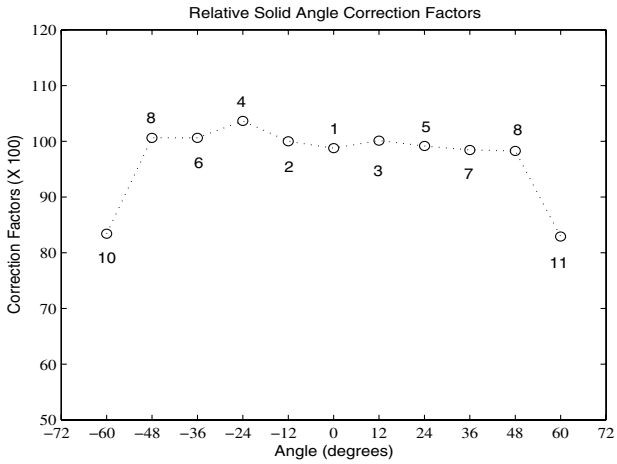

Fig. 4. Relative normalization factors (in %) obtained from the ^{239}Pu α source. The α-particle yields were normalized to telescope 2. The number labels attached to the data points represented by circles indicate the telescope number. Beam-left telescopes are even-numbered and the beam-right ones are odd-numbered.

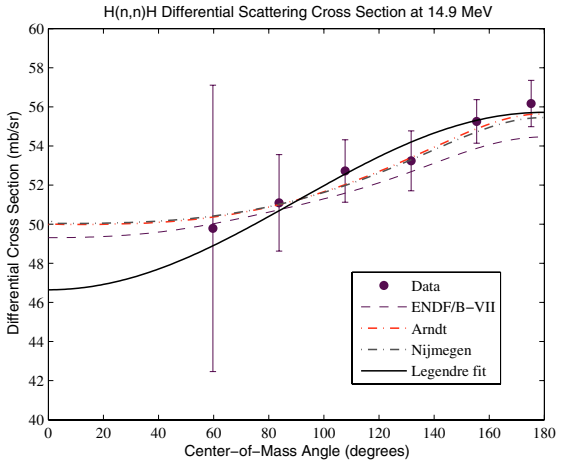

Fig. 5. H(n,n)H differential cross section at a neutron energy of 14.9 MeV compared to the predictions of Nijmegen, Arndt and the ENDF/B-VII evaluation.

with slit-shaped collimators with rounded edges mounted in the vertical plane to diminish the important kinematic spread observed at this angle at the expense of a reduced solid angle as seen in figure 4. Dead time corrections were negligible and amounted to less than 0.1%. Counting losses due to multiple scattering in the target and in the ΔE detector and finite size effects were estimated with a Monte Carlo calculation as described in ref. [1]. They were significant for the 48° and 60° angles. Relativistic kinematics were used to calculate the center-of-mass (CM) relative angular distribution.

3.3 Results and discussion

The (CM) relative angular distribution was fitted with a Legendre polynomial, integrated and normalized to the accurately known total elastic cross section value $\sigma_{\rm el}^{\rm tot} = 643.159$ mb of ref. [5] to obtain the absolute angular distribution values listed in table 1 and shown in figure 5. This absolute angular distribution was then compared to the predictions of Arndt [3], Nijmegen [4] models and to the ENDF/B-VII evaluation [5] using the quantity defined by equation (1):

$$\chi^2 = \frac{1}{N-1}\sum_{i=1}^{N}\left(\frac{\sigma_i^{\exp eriment} - \sigma_i^{\mathrm{mod}\,el}}{\Delta\sigma_i}\right)^2. \qquad (1)$$

$\Delta\sigma_i$ is the experimental uncertainty, N the number of points, and the σ_i are the cross sections. The results are shown in table 2 and indicate a better agreement of the data, in its present state, with the Arndt and Nijmegen predictions than with the ENDF/B-VII evaluation. However, given the small differences between the predictions and the magnitude of the uncertainties in the data, it cannot be concluded with confidence that that is the case. A new experimental run is planned for the very near future to improve statistics and reach the precision required for a more definitive conclusion.

The uncertainties listed in table 1 are essentially statistical in nature. The background was the second most important source of uncertainties for the forward CM direction (60°, 84° and 108°) and was insignificant at the other angles.

Table 1. Absolute values of the measured angular distribution obtained after normalization to the total elastic cross section. $\langle\theta_{\rm cm}\rangle$ is the mean CM neutron scattering angle in degrees.

$\langle\theta_{\rm cm}\rangle$ (°)	$\sigma(\theta_{\rm cm})$ (mb/sr)	Uncertainty (%)
175.24	56.17	2.15
155.47	55.26	2.05
131.65	53.24	2.95
107.72	52.72	3.08
83.75	51.09	4.86
59.72	49.78	14.90

Table 2. Summary of a comparison of the data to the theoretical predictions of Arndt, Nijmegen and to the ENDF/B-VII evaluation.

Model	χ^2
Arndt	0.101
Nijmegen	0.152
ENDF/B-VII	0.811

Table 3. Level of anisotropy in the angular distribution obtained from the present data and those of Arndt, Nijmegen and the ENDF/B-VII evaluation.

	$\frac{\sigma(180°)}{\sigma(0°)}$
Arndt	1.11
Nijmegen	1.11
ENDF/B-VII	1.10
Present data	1.19 ± 0.18

The final angular distribution exhibits a larger degree of anisotropy than what is predicted by Arndt, Nijmegen and the ENDF/B-VII evaluation. The ratio $\sigma(180°)/\sigma(0°)$ was used to estimate the magnitude of this anisotropy in the data and in the three predictions. The results are shown in table 3. The degree of anisotropy in the present data is 8 to 9% higher than in the predictions. The uncertainty in this anisotropy is dominated by the uncertainty in the 60° data point. It is unfortunately too large to infer any definitive conclusion from this comparison. The data 0° and 180° cross section

Table 4. Parameters of the Legendre polynomial fit.

Parameter	Value
a_0 (mb/sr)	51.181
a_1 (mb/sr)	−4.536
$\sigma_{tot}^{elastic,fit}$(mb)	643.159
Log(χ^2)	0.145

values used in this calculation were those obtained from a Legendre polynomial fit that had an excellent χ^2-per-degree-of-freedom value of 1.15. The parameterization of the CM angular distribution was expressed as:

$$\sigma(\theta_{cm}) = a_0 + a_1P_1 + a_2P_2 + a_3P_3 + a_4P_4. \quad (2)$$

The P_i's are the Legendre polynomials of order i. However, the uncertainty in the 60° data point was too large to effectively constrain the fit in the forward CM direction, which limited the highest practical polynomial order for a physically reasonable fit to 1. Higher orders gave a better reduced χ^2 but resulted in un-physical fits in the forward direction. The fit was further limited by the number of degrees of freedom and could not use polynomial orders higher than 4. In comparison, the ENDF/B-VII evaluation uses a polynomial of order 6. The results of the fit are listed in table 4 and shown in figure 5. The difference between the fitted total elastic cross section value and the ENDF/B-VII one was 0.8 μb.

4 Conclusions

The H(n,n)H angular distribution was measured at 14.9 MeV neutron energy with a larger angular range than in any previous measurement. Initial assessment of these data indicates a better agreement with the Arndt and Nijmegen theoretical predictions than with the ENDF/B-VII evaluation. The degree of anisotropy found in the angular distribution was higher than those of the predictions, but, with a large related uncertainty due essentially to the 60° data point. Definitive confirmation of these conclusions requires a further reduction of the statistical uncertainties.

The authors wish to thank Don E. Carter for his help with the electronics and data acquisition systems, John E. O'Donnell for his help with accelerator operations and Devon Jacobs for maintaining the accelerator. Additional thanks to Arjan Plompen of IRMM for the loan of the tritium target.

References

1. N. Boukharouba, F.B. Bateman, C.E. Brient, A.D. Carlson, S.M. Grimes, R.C. Haight, T.N. Massey, O.A. Wasson, Phys. Rev. C **65**, 014004 (2002).
2. F.B. Bateman, S.I. Al-Quraishi, C.E. Brient, N. Boukharouba, A.D. Carlson, S.M. Grimes, R.C. Haight, T.N. Massey, R.T. Wheeler, in *Proc. Int. Conf. on Nuclear Data for Science and Technology*, Santa Fe, 2005, edited by R.C. Haight et al., AIP Conf. Proc. **769**, 834 (2005).
3. R.A. Arndt, I.I. Strakovsky, R.L. Workman, Phys. Rev. C **50**, 2731 (1994).
4. J.J. de Swart, R.A.M.M. Klomp, M.C.M. Rentmeester, Th.A. Rijken, Few-Body Syst., Suppl. **8**, 438 (1995).
5. M.B. Chadwick, P. Oblozinky, M. Hermann et al., *ENDF/B-VII.0: Next Generation Evaluated Nuclear Data Library for Nuclear Science and Technology*, Nucl. Data Sheets **107**, 2931 (2006).